

Submitted to
Phys. Rev.

LBL-1947
Preprint *c. d.*

THEORETICAL X-RAY TRANSITION PROBABILITIES FOR
HIGH Z SUPER-HEAVY ELEMENTS

R. Anholt and J. O. Rasmussen

RECEIVED
LAWRENCE
RADIATION LABORATORY

OCT 9 1973

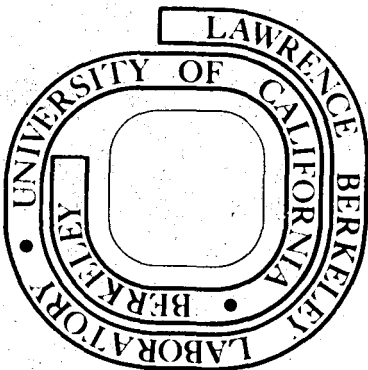
LIBRARY AND
DOCUMENTS SECTION

July 1973

Prepared for the U. S. Atomic Energy Commission
under Contract W-7405-ENG-48

TWO-WEEK LOAN COPY

*This is a Library Circulating Copy
which may be borrowed for two weeks.
For a personal retention copy, call
Tech. Info. Division, Ext. 5545*



34c

LBL-1947
c. d.

DISCLAIMER

This document was prepared as an account of work sponsored by the United States Government. While this document is believed to contain correct information, neither the United States Government nor any agency thereof, nor the Regents of the University of California, nor any of their employees, makes any warranty, express or implied, or assumes any legal responsibility for the accuracy, completeness, or usefulness of any information, apparatus, product, or process disclosed, or represents that its use would not infringe privately owned rights. Reference herein to any specific commercial product, process, or service by its trade name, trademark, manufacturer, or otherwise, does not necessarily constitute or imply its endorsement, recommendation, or favoring by the United States Government or any agency thereof, or the Regents of the University of California. The views and opinions of authors expressed herein do not necessarily state or reflect those of the United States Government or any agency thereof or the Regents of the University of California.

THEORETICAL X-RAY TRANSITION PROBABILITIES FOR HIGH Z SUPER-HEAVY ELEMENTS*

R. Anholt[†]

Department of Chemistry and
Yale Heavy Ion Accelerator Laboratory
Yale University
New Haven, Connecticut 06520

and

J. O. Rasmussen[‡]

Department of Chemistry and
Lawrence Berkeley Laboratory
University of California
Berkeley, California 94720

July 1973

ABSTRACT

K and L x-ray transition probabilities have been calculated for several elements between $Z = 92$ and $Z = 170$. The calculations include multipoles higher than $E1$, are relativistic, and utilize Dirac Hartree-Fock wavefunctions with finite size nuclei. At these very high atomic numbers, many transition rates go through a maximum with Z and other transitions show a maximum and a minimum, and then begin to increase again past $Z = 150$.

I. INTRODUCTION

Of late, considerable interest has developed in x-ray transitions in elements of very high Z . While nuclei with Z greater than 130 are probably so unstable that such transitions can never be observed experimentally in the stationary atom, there is a possibility of observing united-atom x-rays during a collision between a high energy ion and a neutral atom.

In this respect we mention work of Mokler, Stein and Armbruster¹ who claim to have observed M x-rays of $Z = 132, 143, \text{ and } 145$ during a 10 - 60 MeV I bombardment of Au, Th, and U targets. With new heavier ion capabilities of several accelerators throughout the world, there is the possibility of carrying such experiments further to see evidence of M, L, or K shell transitions up to united atom total charge as high as 190. Therefore, it seemed of value to us to carry out theoretical calculations of radiative transition rates for very high atomic numbers.

Previously there have been almost no transition probabilities calculated for any element above $Z = 93$, though a considerable number have been made for elements below that atomic number. The earliest relativistic calculations were done by Payne and Levinger² and later Payne and Taylor³ who employed analytical Dirac wavefunctions with screening to calculate K transition rates in a number of elements up through lead. F. A. Babuskin⁴ similarly used analytical Dirac wavefunctions, but in addition, he used less approximate expressions for the electric and magnetic multipole fields, and he even investigated the inclusion of finite nuclear size in his calculations. His work, while being analytically more elegant than subsequent work, has largely been superseded by approaches which use computer-calculated Hartree-Fock many electron wavefunctions instead of one-electron Dirac functions.

Among these are the calculations of three groups, Rosner and Bhalla,⁵ Scofield,⁶ and Lu, Malik and Carlson.⁷ We have followed their approach closely herein and we discuss it below.

II. RELATIVISTIC FORMULATION OF TRANSITION RATES

As usual for quantum mechanical transition probabilities we begin with the Fermi Golden rule, writing the transition rate ω as

$$\omega = 2\pi S | \langle f | H_{int} | i \rangle |^2 \rho(E_f) \quad (1)$$

where S stands for the summation over final and average over initial states, and we have taken atomic units throughout ($\hbar = m = e = 1$). H_{int} , in this analysis will be taken as:

$$H_{int} = \sum_{i=1}^N \tilde{J}_i \cdot \tilde{A} \quad (2)$$

with $\tilde{J} = c\tilde{\alpha}$, $\tilde{\alpha}$ being the usual Dirac matrix. For the \tilde{A} field we take the sum over electric and magnetic multipoles expressed as:

$$A_{L,M}^{(e)} = \sqrt{\frac{4\pi\omega}{R}} \left\{ \sqrt{\frac{L+1}{2L+1}} j_{L-1}(\omega r) T_{L,L-1}^M(\theta,\phi) - \sqrt{\frac{L}{2L+1}} j_{L+1}(\omega r) T_{L,L+1}^M(\theta,\phi) \right\} \quad (3)$$

$$\text{and } A_{L,M}^{(m)} = \sqrt{\frac{4\pi\omega}{R}} \left\{ -j_L(\omega r) \cdot T_{L,L}^M(\theta,\phi) \right\}$$

with $j_L(\omega r)$ the spherical Bessel functions of the first kind and $T_{L,L}^M$ spherical tensors defined by Rose.⁸

The wavefunctions in this analysis can be expressed as:

$$\psi_{\kappa}^{\mu} = \begin{pmatrix} G/r & \chi_{\kappa}^{\mu} \\ iF/r & \chi_{-\kappa}^{\mu} \end{pmatrix} \quad (4)$$

where κ is the usual relativistic quantum number ($\kappa = \ell$ for $\kappa > 0$, $\kappa = -\ell - 1$ for $\kappa < 0$). Performing the necessary algebra, we then have for the magnetic and electric transition rates between final and initial states labelled with and without a prime, respectively:

$$\begin{aligned} \omega_{\kappa\kappa'}^{(ML)} &= 2 \omega (\kappa + \kappa')^2 [(2\bar{\ell}' + 1)(2\ell + 1)(2j' + 1)/L(L+1)] \\ &\times C^2(\ell\bar{\ell}'L; 000) W^2(j\ell j'\bar{\ell}'; \frac{1}{2}L) \cdot \left[\int_0^{\infty} (G_{\kappa\kappa'} F_{\kappa\kappa'} + F_{\kappa\kappa'} G_{\kappa\kappa'}) j_L(\omega r) dr \right]^2 \\ \omega_{\kappa\kappa'}^{(EL)} &= 2 \omega [(2\ell' + 1)(2\ell + 1)(2j' + 1)/(2L+1)^2] C^2(\ell\ell'L; 000) W^2(j\ell j'\ell'; \frac{1}{2}L) \\ &\times \left\{ \sqrt{\frac{L+1}{L}} \int_0^{\infty} \left\{ (\kappa' - \kappa)(G_{\kappa\kappa'} F_{\kappa\kappa'} + F_{\kappa\kappa'} G_{\kappa\kappa'}) + L(G_{\kappa\kappa'} F_{\kappa\kappa'} - F_{\kappa\kappa'} G_{\kappa\kappa'}) \right\} j_{L-1}(\omega r) dr \right. \\ &\left. - \sqrt{\frac{L}{L+1}} \int_0^{\infty} \left\{ (\kappa' - \kappa)(G_{\kappa\kappa'} F_{\kappa\kappa'} + F_{\kappa\kappa'} G_{\kappa\kappa'}) - (L+1)(G_{\kappa\kappa'} F_{\kappa\kappa'} - F_{\kappa\kappa'} G_{\kappa\kappa'}) \right\} j_{L+1}(\omega r) dr \right\}^2 \end{aligned} \quad (5)$$

where α is the fine structure constant, $\omega = \alpha(E_f - E_i)$ in atomic units, and $\bar{\ell}'$, in the notation introduced by Rose⁹ is taken as $-\kappa'$ for $\kappa' < 0$ or $\kappa' - 1$ for $\kappa' > 0$.

We mention at this point that the choice of the field here is arbitrary and we could just as well, following Scofield, have taken for the electric field the following:

$$A_{LM}^{(e)} = \sqrt{\frac{4\pi\omega}{R}} (L(L+1))^{-1/2} \vec{\nabla} \times \vec{L} j_L(\omega r) Y_{LM}(\hat{r})$$

in which case we would obtain for the transition rate

$$\omega_{KK'}(EL) = 2 \omega [(2\ell'+1) (2\ell+1) (2j'+1)/L(L+1)] c^2(\ell\ell'L;000) W^2(j\ell j'\ell'; \frac{1}{2} L) \times \left[\int_0^\infty dr \left\{ j_{L-1}(\omega r) [(\kappa'-\kappa) (F_{\kappa\kappa'} G_{\kappa\kappa'} + G_{\kappa\kappa'} F_{\kappa\kappa'}) - L(F_{\kappa\kappa'} G_{\kappa\kappa'} - G_{\kappa\kappa'} F_{\kappa\kappa'})] + L(G_{\kappa\kappa'} G_{\kappa\kappa'} + F_{\kappa\kappa'} F_{\kappa\kappa'}) j_L(\omega r) \right\} \right]^2 \quad (6)$$

The details of the relativistic Hartree-Fock-Slater (RHFS) calculations used by Bhalla, Scofield, and by Lu, Malik, and Carlson do not differ by very much. They all employ the usual Slater approximation to the exchange term:

$$V_s = \frac{3\alpha}{2\pi} [3\pi^2 p(r)]^{1/3}$$

and with the exception of Scofield's calculation, they take account of finite nuclear size (though in various different ways) For our calculations, we have used wavefunctions from J.B.Mann at the Los Alamos Scientific Laboratory. These wavefunctions are based on a Dirac-Hartree-Fock (DHF) Code¹⁰ which calculates the many two-electron exchange integrals exactly. The finite nuclear size is taken as a two parameter Fermi distribution with $R = 1.07A^{1/3}$ fm, $a = 1.0393 \times 10^{-5}$ au, and $A = 3Z-46$. More sophisticated extrapolations for A yielded results which were not too much different from those used in this calculation.¹¹

For the matrix elements necessary to calculate transition probabilities, we integrated along the same exponential radial grid as was used to calculate the self-consistent field. In such a grid each r_i is given as $r_i = r_0 e^{hi}$ with $r_0 = 5 \times 10^{-5}$ au and h is selected to give a maximum radius of 40 a.u. at $i = 421$. We found that interpolating the wavefunctions at linear intervals of .001, 0.01, and 0.00001 a.u. when the exponential grid was wider than this did not change the value of the matrix elements by more than .5%.

For the x-ray transition energy, we have taken the difference between Mann's eigenvalues. Lu, Malik and Carlson^{7,12} examined the error associated with this approximation for $Z = 92$ and 126. They used experimental data extrapolating a curve that goes approximately as Z^4 up to $Z = 126$, to find the correction due to quantum electrodynamic and other terms. When this correction was applied to the differences between eigenvalues, and the x-ray transition probabilities were recalculated, the difference in the rates was on the order of 0.1%. The difference between the energies was around .5%, and we note from extrapolating the curves even further, that this does not become much greater as one approaches $Z = 200$.

We mention one other source of error and that is in not taking the initial and final wavefunctions with a hole in the appropriate shells. The wavefunctions we have taken are for the neutral atoms. Lu, Malik, and Carlson have examined this source of error for $Z = 92$ and 126 K x-ray transition rate calculations. They found the difference in the transition rates to be on the order of 1 or 2%, the hole wavefunction rates giving consistently higher rates. Again, however, these do not become drastically larger than 1 or 2% as one goes to higher Z . Furthermore, it is not to be expected that ionization of shells

outside the shells involved in the transition will much affect the rate. As the work of Watson and Rasmussen¹³ showed, the K x-ray energies were hardly affected by extensive ionization in fission fragments, and by the same token removal of outershell electrons will not much affect innershell wavefunctions.

III. NUMERICAL RESULTS

Table I gives a comparison between transition rates for $Z = 92$ and 126 calculated by Bhalla, by Scofield, by Lu, Malik, and Carlson, and by ourselves. The units used throughout are atomic rate units ($1 \text{ au} = 4.132 \times 10^{18} \text{ sec}^{-1}$). In all cases, these four agree within a few percent.

One would like to compare these calculated transition rates with experimental quantities. Of course, this is at present impossible with the super-heavy elements. However, it is possible to make comparisons with experimental data for the lighter elements. Scofield has compared the total K emission rates with experimental quantities for 10 elements between $Z = 16$ and 79 , and the agreement appeared to be within the experimental uncertainties. Ratios between various line intensities may also be compared, as is done for various K and L transitions in Table II. Even here, the agreement is fairly good, though some of the L ratios are off by as much as 20%.

Figure 1 is a plot of the transition rate vs. Z for $K-L_2$ and $K-L_3$ (K_{α_2} and K_{α_1}) transitions and compares our calculations with Lu, Malik, and Carlson's (the two curves cannot be resolved on the plot). Also plotted are our calculations made using analytical one electron Dirac wavefunctions found in Ref. 9 (assuming a point nucleus, no screening, and using Eq. (5)). Note the sharply decreasing behavior of the transition rates calculated with analytical Dirac wavefunctions as Z approaches 137 , and those calculated with DHF

wavefunctions as Z approaches 170. [‡] This behavior can be explained in the following way: As one approaches a stronger central field, the $1s$ wavefunction is pulled in closer and closer toward the nuclear center, while the L and M shell wavefunctions are not pulled in as fast. This means that the overlap between the K and other shell wavefunctions will begin to decrease, as will the integral over the overlap and spherical Bessel function, and hence the transition rate. Indeed, if one examines the integrals over the appropriate spherical Bessel functions in Eq. (5), it is evident that this is exactly what is happening.

Many other transition rates show this same maximal behavior. Table III gives a summary of our calculated radiative rates for filling vacancies in the K , L_1 , L_2 , and L_3 shells, and from this table, figures 2 through 7 were drawn to illustrate the predicted K x-ray spectra of these super heavy elements. The two lowest multiplicities are taken into account; for at high Z , the electric dipole rates are no longer predominant over other multipoles. We have noted the occurrence of a maximum in the $K-L_2$ and $K-L_3$ rates, but other transition rates show an even more surprising behavior. For instance, the M_2 to K transition reaches a maximum at 130, decreases by two orders of magnitude, then starts to rise again and keeps rising up to $Z = 170$. The N_2 to K transition does the same, as do the M_3-L_1 , N_3-L_1 , M_1-L_2 , N_1-L_2 , and N_1-L_3 transitions.

IV. DISCUSSION

What is the explanation for this extreme variation of rates with Z ? We can see that the rate minima never occur for transitions between states both without radial nodes. Let us examine the details of contributions to the M_2 to K transition. We have ascertained three particular aspects: a) that the entire quantity inside brackets in Eq. (5) changes sign between $Z = 130$ and

$Z = 150$; b) that if one computes the moments of r , i.e., $\int G_K G_K r dr$ and $\int F_K F_K r dr$, these two also switch signs between $Z = 130$ and $Z = 150$; finally, c) all of the results are unaffected if one uses Eq. (6) instead of Eq. (5).

The difference in the calculated transition rates are only a few percent at most.

The significance of the second point (b) is that it is the integral $\int G_K G_K r dr$ that must be calculated to determine the dipole matrix element for the transition "non-relativistically", i.e., by taking the non-relativistic wavefunctions approximately as the major component G_K . Figure 8 shows a plot of $G_{3p-} \times G_{1s} \times r$

vs. r and indicates why this change of sign occurs. The product has one node, and as the $1s$ wavefunction is pulled in closer and closer to the nucleus at higher Z , the area under the positive lobe decreases with respect to that under the negative lobe. The wavefunction G_{3p+} has a node as does the $3p-$ wavefunction, so it is fair to ask why this same behavior does not occur there also. Figure 9 shows why. The node occurs at a larger value of r , where the G_{1s} wavefunction is much smaller; hence, the negative lobe of the product function is not as large as in the $3p-$ case.

With these observations, it is not hard to see why the entire quantity inside the brackets in Eq. (5) changes signs also, as one goes from $Z = 130$ to $Z = 150$.

Lastly, it is interesting to speculate on the experimental observability of these transition rates at high Z . It is unfortunate that the kinds of united atom collisional radiation experiments that we mentioned earlier do not yield discrete peaks in x-ray spectra. Instead, one can only hope to observe a continuum extending from the x-ray peak of the heavier atom down to an endpoint which would correspond to the $K_{\beta_2}^{16}$ transition energy of the united atom (UA).

Previous experiments have not been able to unfold radiative lifetimes out of UA x-ray yields, due mostly to the complicated nature of the electron promotion processes going on inside their targets, and a myriad of other factors.

We would hope ultimately that the maximum total K rate behavior as shown in Fig. 4 might be reflected in the yield and spectral shape curves as united atom K x-ray studies are pushed from the present limit of $Z_{UA} = 70$ of Meyerhof et al.,¹⁶ on up to $Z_{UA} \geq 140$.

Of course much more research is needed on relativistic two-center molecular orbitals and other aspects of united atom x-ray production. It is hoped that this paper will stimulate these kinds of research.

V. ACKNOWLEDGMENTS

This work was supported by the A.E.C. through the Yale Heavy Ion Accelerator Contract. The authors wish to thank Joe Mann at the Los Alamos Scientific Laboratory for sending us the wavefunctions used in this calculation and the Department of Computer Sciences at Yale University for the free use of their PDP-10 computer. In addition, one of us (RA) acknowledges fruitful discussions with Donald Beck in the Chemistry Department at Yale University.

FOOTNOTES AND REFERENCES

- * Work performed under the auspices of the U. S. Atomic Energy Commission.
- † Present address: University of California, Lawrence Berkeley Laboratory, Berkeley, California
- ‡ J. S. Guggenheim Fellow, 1973.
- ‡ Mann reports that the K binding energy falls into the positron sea at $Z = 172$.¹¹
1. P. H. Mokler, H. J. Stein, and P. Armbruster, Phys. Rev. Letters 29, 827 (1972).
 2. W. B. Payne and J. S. Levinger, Phys. Rev. 101, 1020 (1956).
 3. G. R. Taylor and W. B. Payne, Phys. Rev. 118, 1549 (1960).
 4. F. A. Babuskin, JETP 21, 372 (1965; Acta Physica. Polon 25, 749 (1964), 31, 459 (1967)).
 5. H. R. Rosner and C. P. Bhalla, Z. Phys. 231, 347 (1970).
 6. James Scofield, Phys. Rev. 179, 9 (1969).
 7. C. C. Lu, F. B. Malik, and T. A. Carlson, Nucl. Phys. A175, 289 (197-).
 8. M. E. Rose, Elementary Angular Momentum (John Wiley & Sons, New York, 1957).
 9. M. E. Rose, Relativistic Electron Theory (John Wiley & Sons, New York, 1956).
 10. J. B. Mann and J. T. Waber, J. Chem. Phys., 53, 2397 (1970); Atomic Data, 5, 201 (1973).
 11. J. B. Mann, private communication.
 12. T. A. Carlson, C. W. Nestor, F. B. Malik, and T. C. Tucker, Nucl. Phys. A135, 57 (1969).
 13. R. L. Watson and J. O. Rasmussen, J. Chem. Phys. 47, 778 (1967).
 14. S. I. Salem and C. W. Schultz, Atomic Data 3, 215 (1971).

15. G. C. Nelson, B. G. Saunders, and S. I. Salem, Atomic Data 1, 377 (1970).
16. W. E. Meyerhof, T. K. Saylor, S. M. Lazarus, W. A. Little, B. B. Triplett, and L. F. Chase, Jr., Phys. Rev. Letters 26, 1279 (1973).

Table I. Comparison of K-Shell Radiative Transition Rates for $Z = 92$ and 126 .

Author	K-L _I	K-L _{II}	K-L _{III}	K-M _{II}	K-M _{III}	K-M _{IV}	K-M _V	K-N _{II}	K-N _{III}	K-N _{IV}	K-N _V
$Z = 92$											
Bhalla ^a	0.0043	1.056	1.681	0.194	0.381	0.00697	0.0079	0.049	0.099	0.0021	0.0024
Scofield ^d	0.0038	1.01	1.622	0.187	0.366	0.0065	0.0075	0.047	0.095	0.0041	0.0041
LMC ^c	-	1.01	1.62	0.187	0.366	0.0065	0.0074	0.047	0.095	0.0019	0.0022
This work	0.0037	1.005	1.602	0.186	0.362	0.00644	0.0073	0.046	0.093	0.0019	0.0022
$Z = 126$											
LMC ^c	-	3.71	4.66	0.495	1.23	0.037	0.030	0.124	0.373	0.0133	0.0116
This work ^b	0.19(0.01)	3.6	4.6	0.485	1.22	0.037	0.031	0.12	0.37	0.0133	0.0115

^aResults are for $Z = 93$, so they are consistently higher than others, Ref. 5.

^bInterpolated.

^cRef. 7.

^dRef. 6.

Table II. Comparison of Intensity Ratios with Experiment for $Z = 92$.

Ratio	Experiment ^a	This work	Scofield
$K_{\alpha_2}/K_{\alpha_1}$	0.624	0.627	0.623
L_{β_3}/L_{β_1}	0.548	0.513	0.510
$(K_{\beta_1} + K_{\beta_3})/K_{\alpha_1}$	0.354	0.342	0.341
$K_{\beta_1}^{\wedge}/K_{\alpha_1}$	0.363	0.351	0.350
$K_{\beta_2}^{\wedge}/K_{\alpha_1}$	0.123	0.0861 ^b	0.087 ^b
K_{β}/K_{α}	0.299	0.272 ^b	0.270 ^b
L_{β_4}/L_{β_3}	1.10	1.15	1.15
L_{γ_3}/L_{β_3}	0.438	0.310	0.310
L_{γ_2}/L_{β_3}	0.402	0.308	0.313
L_{η}/L_{β_1}	0.0280	0.0286	0.0284
L_{γ_1}/L_{β_1}	0.240	0.226	0.226
$L_{\beta_{2,15}}/L_{\alpha_1}$	0.275	0.233	0.233
$L_{\alpha_2}/L_{\alpha_1}$	0.110	0.114	0.114
L_{β_6}/L_{β_1}	0.0185	0.0175	0.0174

^aExperimental data taken from a recent compilation by Salem and Schultz¹⁴ and Nelson, Saunders, and Schultz.¹⁵ X-ray notation used here is explained therein. The estimated experimental uncertainties ranged from 3 to 10%.

^bIncluded in $K_{\beta_2}^{\wedge}$ and K_{β} are transitions from higher levels that were not calculated theoretically.

Table IIIa. K Transition Rates (au).

	L1	L2	L3	M1	M2	M3	M4
Z	M1	E1	E1/M2	M1	E1	E1/M2	E2/M1
92	0.3734(-2)	0.1005(1)	0.1602(1)	0.1196(-2)	0.1859(0)	0.3619(0)	0.6438(-2)
112	0.4009(-1)	0.2308(1)	0.3234(1)	0.1293(-1)	0.3845(0)	0.7968(0)	0.2028(-1)
130	0.2866(0)	0.4121(1)	0.4955(1)	0.8868(-1)	0.4930(0)	0.1339(1)	0.4117(-1)
150	0.1989(1)	0.4623(1)	0.5779(1)	0.5259(0)	0.2680(-1)	0.1775(1)	0.5684(-1)
160	0.4273(1)	0.2916(1)	0.5315(1)	0.1002(1)	0.1600(0)	0.1755(1)	0.5288(-1)
170	0.7641(1)	0.1440(1)	0.4514(1)	0.1615(1)	0.6219(0)	0.1605(1)	0.4304(-1)
	M5	N1	N2	N3	N4	N5	N6
Z	E2/M3	M1	E1	E2/M2	E2/M1	E2/M3	M2
92	0.7334(-2)	0.3445(-3)	0.4589(-1)	0.9344(-1)	0.1891(-2)	0.2161(-2)	0.1621(-8)
112	0.1984(-1)	0.3981(-2)	0.9895(-1)	0.2285(0)	0.6871(-2)	0.6813(-2)	0.2899(-7)
130	0.3338(-1)	0.2783(-1)	0.1194(0)	0.4126(0)	0.1526(-1)	0.1268(-1)	0.2015(-6)
150	0.3485(-1)	0.1600(0)	0.7280(-3)	0.5837(0)	0.2284(-1)	0.1449(-1)	0.9233(-6)
160	0.2777(-1)	0.2948(0)	0.6433(-1)	0.5955(0)	0.2204(-1)	0.1204(-1)	0.1482(-5)
170	0.1946(-1)	0.4591(0)	0.1799(0)	0.5623(0)	0.1862(-1)	0.8792(-2)	0.1967(-5)

Table IIIb. L1 Transition Rates (au)

	L2	L3	M1	M2	M3	M4
Z	E1	E1/M2	M1	E1	E1/M2	E2/M1
92	0.1114(-5)	0.5026(-2)	0.1790(-5)	0.3103(-1)	0.2698(-1)	0.1477(-2)
112	0.4944(-5)	0.4783(-1)	0.2805(-4)	0.1006(0)	0.3772(-1)	0.7189(-2)
130	0.1857(-2)	0.3417(0)	0.3213(-3)	0.3039(0)	0.9804(-2)	0.2707(-1)
150	0.2597(-1)	0.2430(1)	0.5225(-2)	0.1257(1)	0.1400(0)	0.1043(0)
160	0.2934(0)	0.5168(1)	0.2003(-1)	0.2289(1)	0.6147(0)	0.1831(0)
170	0.1350(1)	0.9057(1)	0.6846(-1)	0.3560(1)	0.1525(1)	0.2913(0)
	M5	N1	N2	N3	N4	N5
Z	E2/M3	M1	E1	E1/M2	E2/M1	E2/M3
92	0.2194(-2)	0.8464(-6)	0.8314(-2)	0.8367(-2)	0.2544(-3)	0.4059(-3)
112	0.1040(-1)	0.1385(-4)	0.2829(-1)	0.1470(-1)	0.1508(-2)	0.2403(-2)
130	0.3655(-1)	0.1598(-3)	0.8273(-1)	0.7513(-2)	0.6879(-2)	0.1031(-1)
150	0.1186(0)	0.2428(-2)	0.2542(0)	0.2601(-1)	0.3266(-1)	0.4078(-1)
160	0.1827(0)	0.8724(-2)	0.3414(0)	0.1540(0)	0.6219(-1)	0.6790(-1)
170	0.2499(0)	0.2783(-1)	0.3737(0)	0.4293(0)	0.1051(0)	0.9892(-1)

Table IIIc. L2 Transition Rates (au)

	L3	M1	M2	M3	M4	M5
Z	E2/M1	E1	M1	E2/M1	E1/M2	M2
92	0.2361(-3)	0.3412(-2)	0.5010(-6)	0.1749(-3)	0.1189(0)	0.1052(-4)
112	0.2396(-3)	0.9882(-2)	0.7851(-5)	0.7169(-3)	0.3020(0)	0.8242(-4)
130	0.3587(-2)	0.2229(-1)	0.9964(-4)	0.2268(-2)	0.5688(0)	0.4421(-3)
150	0.7150(-1)	0.1631(-1)	0.2591(-2)	0.1884(-1)	0.6662(0)	0.2292(-2)
160	0.2440(0)	0.4033(-3)	0.1184(-1)	0.6697(-1)	0.4842(0)	0.3920(-2)
170	0.5435(0)	0.6978(-1)	0.3540(-1)	0.1645(0)	0.3177(0)	0.5001(-2)
	N1	N2	N3	N4	N5	
Z	E1	M1	E2/M1	E1/M2	M2	
92	0.9148(-3)	0.1997(-6)	0.5258(-4)	0.2696(-1)	0.3269(-5)	
112	0.2844(-2)	0.3516(-5)	0.2456(-3)	0.8108(-1)	0.2966(-4)	
130	0.6727(-2)	0.4518(-4)	0.8585(-3)	0.1763(0)	0.1746(-3)	
150	0.5879(-2)	0.1012(-2)	0.6272(-2)	0.2464(0)	0.9703(-3)	
160	0.1260(-4)	0.3941(-2)	0.2192(-1)	0.1938(0)	0.1708(-2)	
170	0.1436(-1)	0.1024(-1)	0.5520(-1)	0.1353(0)	0.2248(-2)	

Table IIIId. L3 Transition Rates (au)

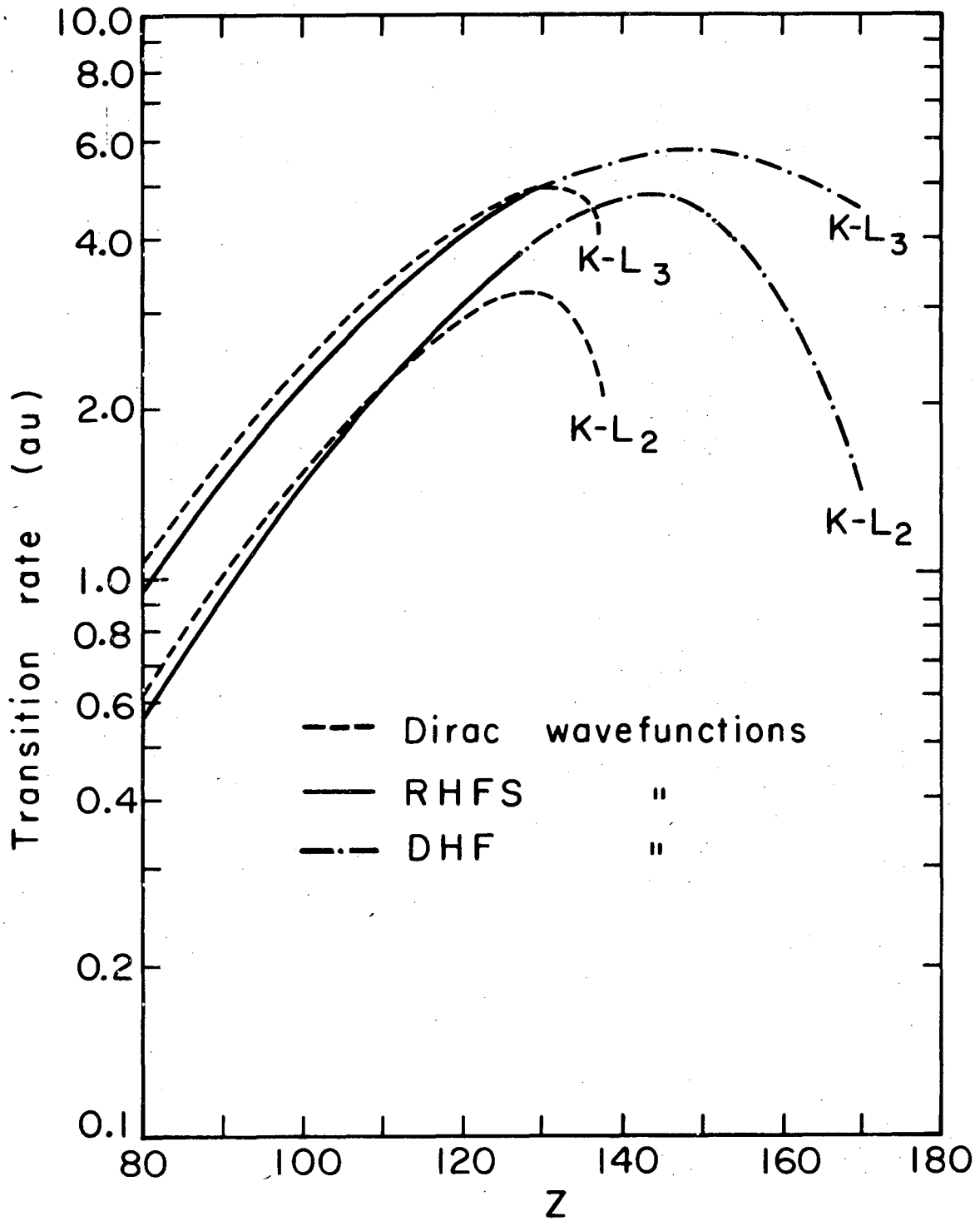
	M1	M2	M3	M4	M5
Z	E1/M2	E2/M1	E2/M1	E1	E1/M2
92	0.6109(-2)	0.8425(-4)	0.7053(-4)	0.1003(-1)	0.8796(-1)
112	0.1999(-1)	0.2730(-3)	0.2724(-3)	0.2378(-1)	0.2076(0)
130	0.4358(-1)	0.5277(-3)	0.7183(-3)	0.4464(-1)	0.3888(0)
150	0.4223(-1)	0.3296(-3)	0.1866(-2)	0.7968(-1)	0.6930(0)
160	0.1829(-1)	0.8503(-1)	0.2872(-2)	0.1027(0)	0.8933(0)
170	0.2044(-2)	0.5894(-2)	0.4398(-2)	0.1302(0)	0.1133(1)

	N1	N2	N3	N4	N5
Z	E1/M2	E2/M1	E2/M1	E1	E1/M2
92	0.1541(-2)	0.1682(-4)	0.1953(-4)	0.2026(-2)	0.1849(-1)
112	0.5079(-2)	0.5022(-4)	0.7883(-4)	0.5223(-2)	0.4917(-1)
130	0.9879(-2)	0.9363(-4)	0.2252(-3)	0.1011(-1)	0.9903(-1)
150	0.4097(-2)	0.8760(-3)	0.6111(-3)	0.1805(-1)	0.1870(0)
160	0.6182(-4)	0.2138(-2)	0.9740(-3)	0.2301(-1)	0.2473(0)
170	0.1122(-1)	0.3536(-2)	0.1535(-2)	0.2866(-1)	0.3218(0)

FIGURE CAPTIONS

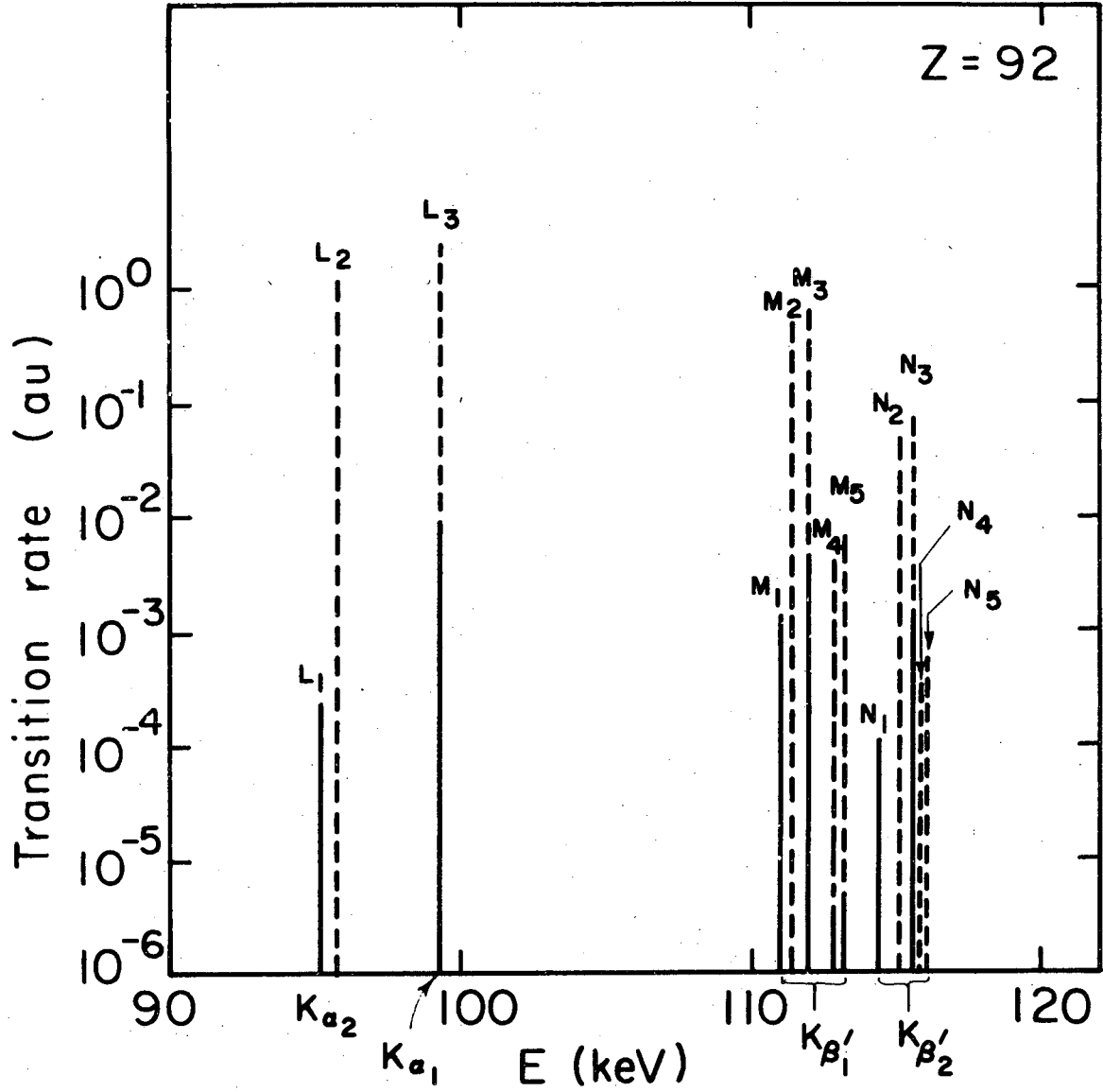
- Fig. 1. $K-L_3$ and $K-L_2$ transition rates vs Z . Calculations made by Lu, Malik, Carlson⁷ using RHFS wavefunctions, and by ourselves, using hydrogenic Dirac wavefunctions and Mann's many electron Dirac-Hartree-Fock wave functions.
- Fig. 2. Transition rate vs E histogram for $Z = 92$. Magnetic contribution to transition rate is drawn as solid line; the remaining contribution is drawn as dashed line. Multipoles calculated are given in Table III.
- Fig. 3. Transition rate vs E histogram for $Z = 112$. Magnetic contribution to transition rate is drawn as solid line; the remaining contribution is drawn as dashed line. Multipoles calculated are given in Table III.
- Fig. 4. Transition rate vs E histogram for $Z = 130$. Magnetic contribution to transition rate is drawn as solid line; the remaining contribution is drawn as dashed line. Multipoles calculated are given in Table III.
- Fig. 5. Transition rate vs E histogram for $Z = 150$. Magnetic contribution to transition rate is drawn as solid line; the remaining contribution is drawn as dashed line. Multipoles calculated are given in Table III.
- Fig. 6. Transition rate vs E histogram for $Z = 160$. Magnetic contribution to transition rate is drawn as solid line; the remaining contribution is drawn as dashed line. Multipoles calculated are given in Table III.
- Fig. 7. Transition rate vs E histogram for $Z = 170$. Magnetic contribution to transition rate is drawn as solid line; the remaining contribution is drawn as dashed line. Multipoles calculated are given in Table III.
- Fig. 8. Major component of the $3p_{1/2} (M_2)$ wavefunction multiplied by that for the $1s$ times r vs r for $Z = 130$ and $Z = 150$. Note the relative magnitude of the positive and negative lobes.

Fig. 9. Major component of the $3p_{3/2} (M_3)$ wavefunction multiplied by that for the $1s$ times r vs r for $Z = 130$ and $Z = 150$. Note the relative magnitude of the positive and negative lobes.



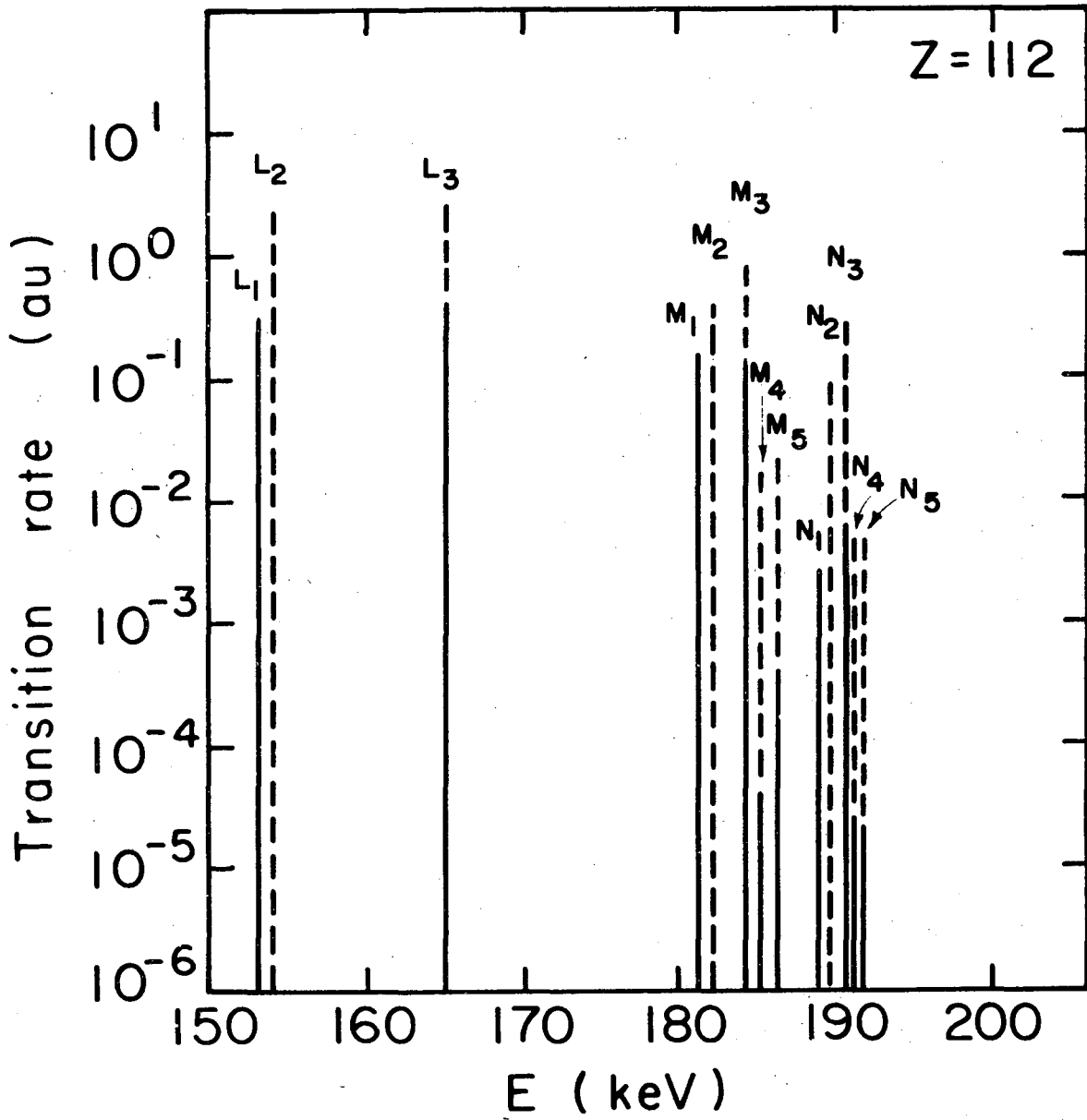
XBL738-3716

Fig. 1



XBL738-3722

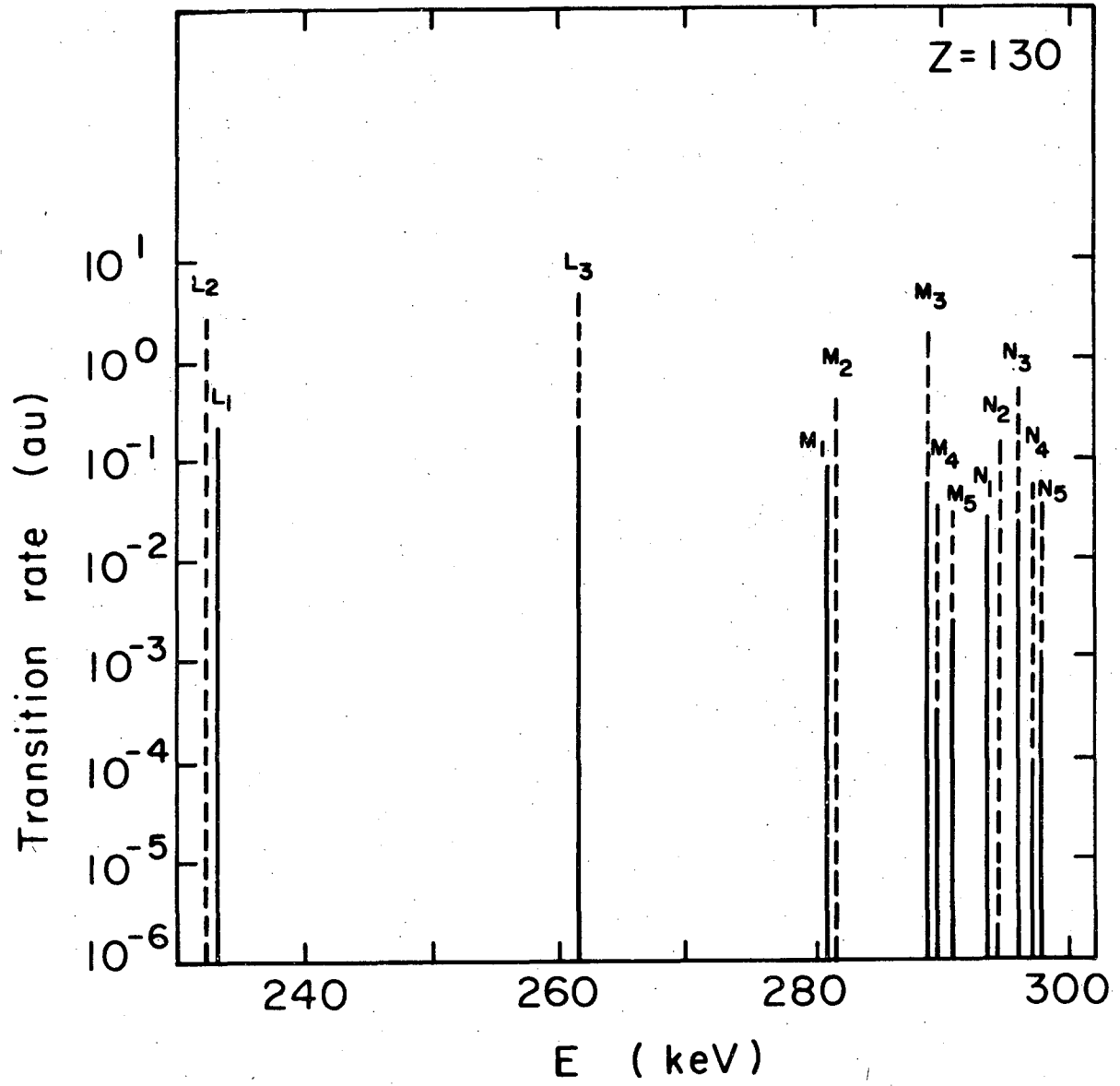
Fig. 2



XBL 738-3721

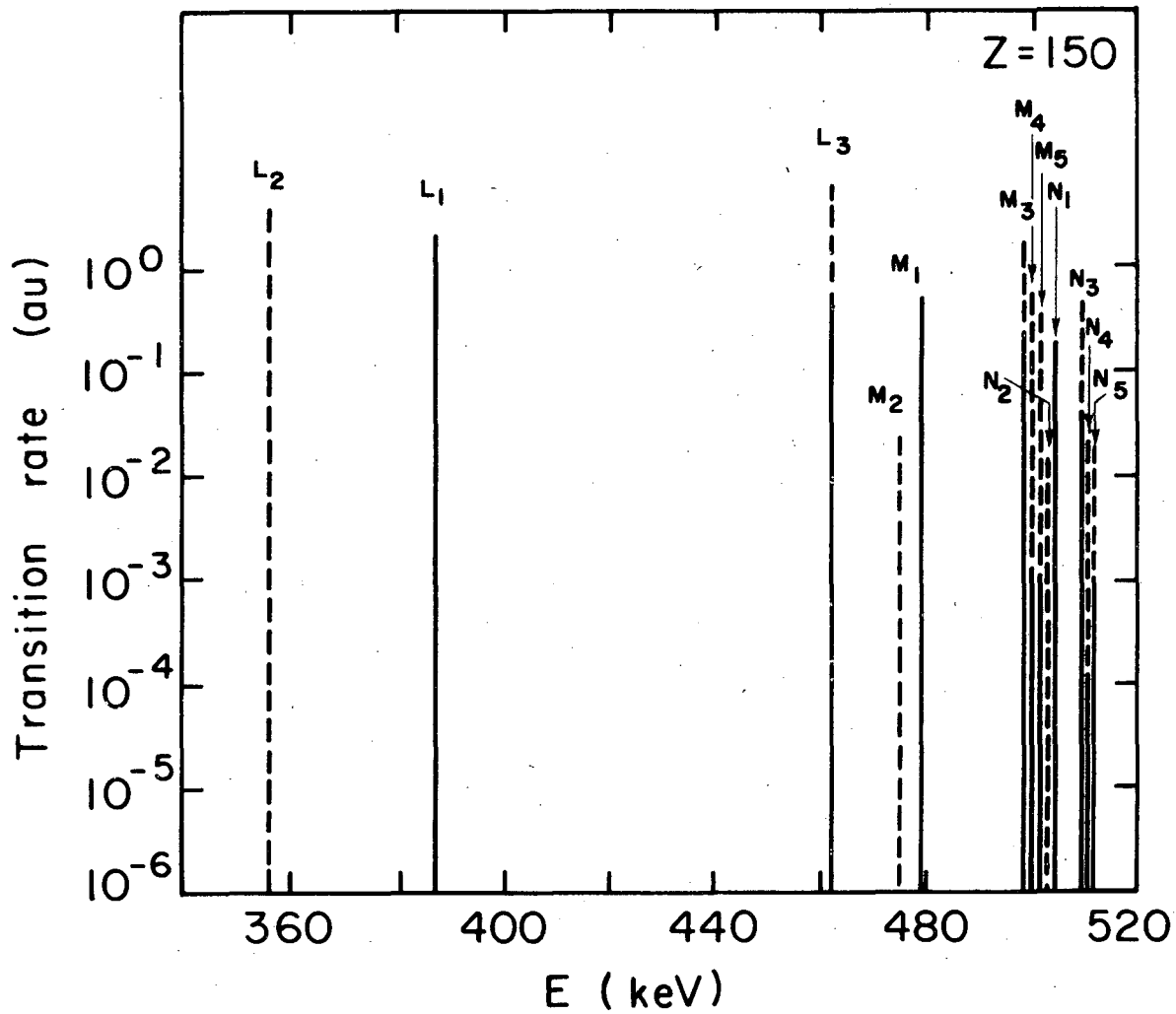
Fig. 3

e



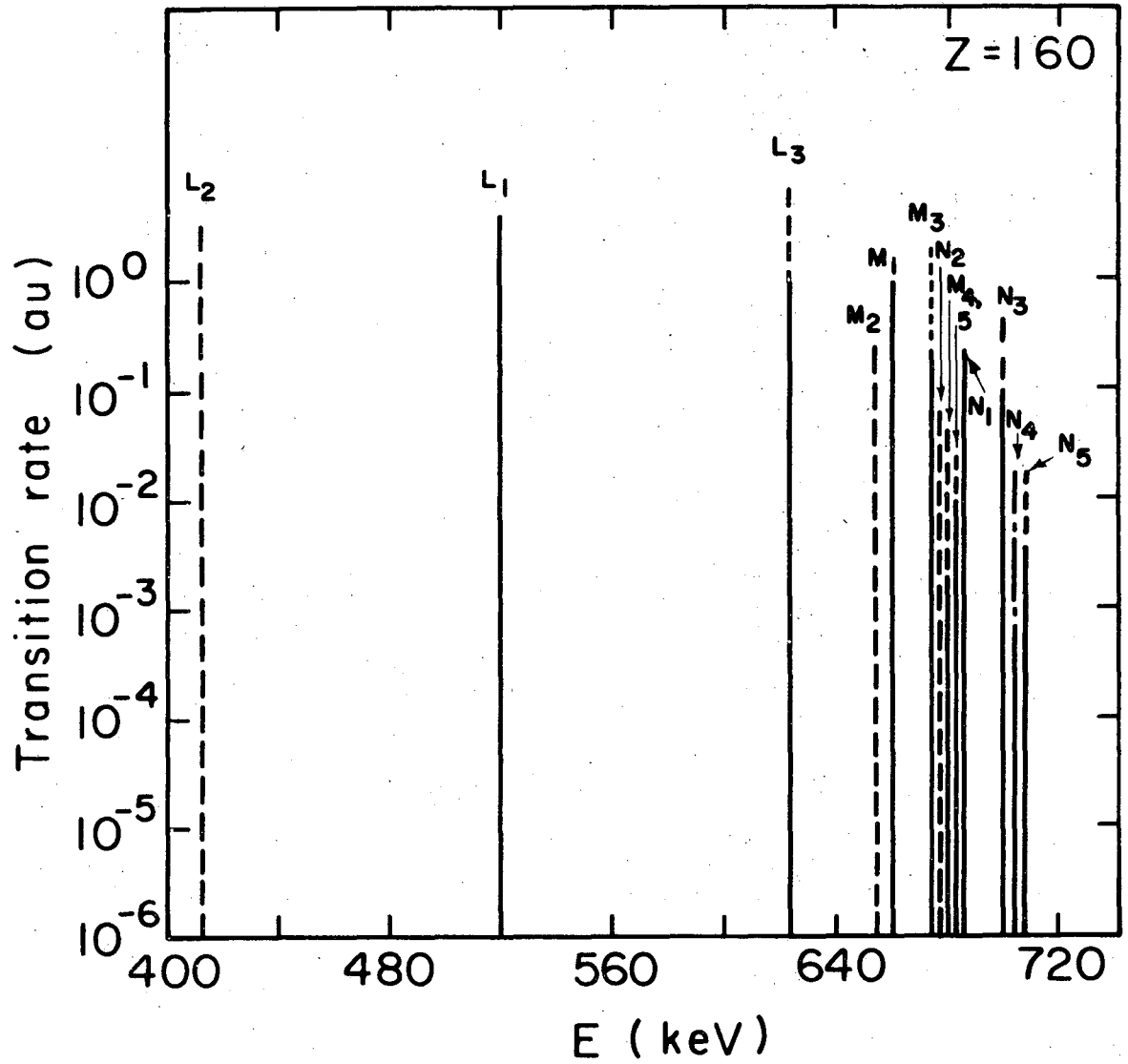
XBL 738 - 3720

Fig. 4



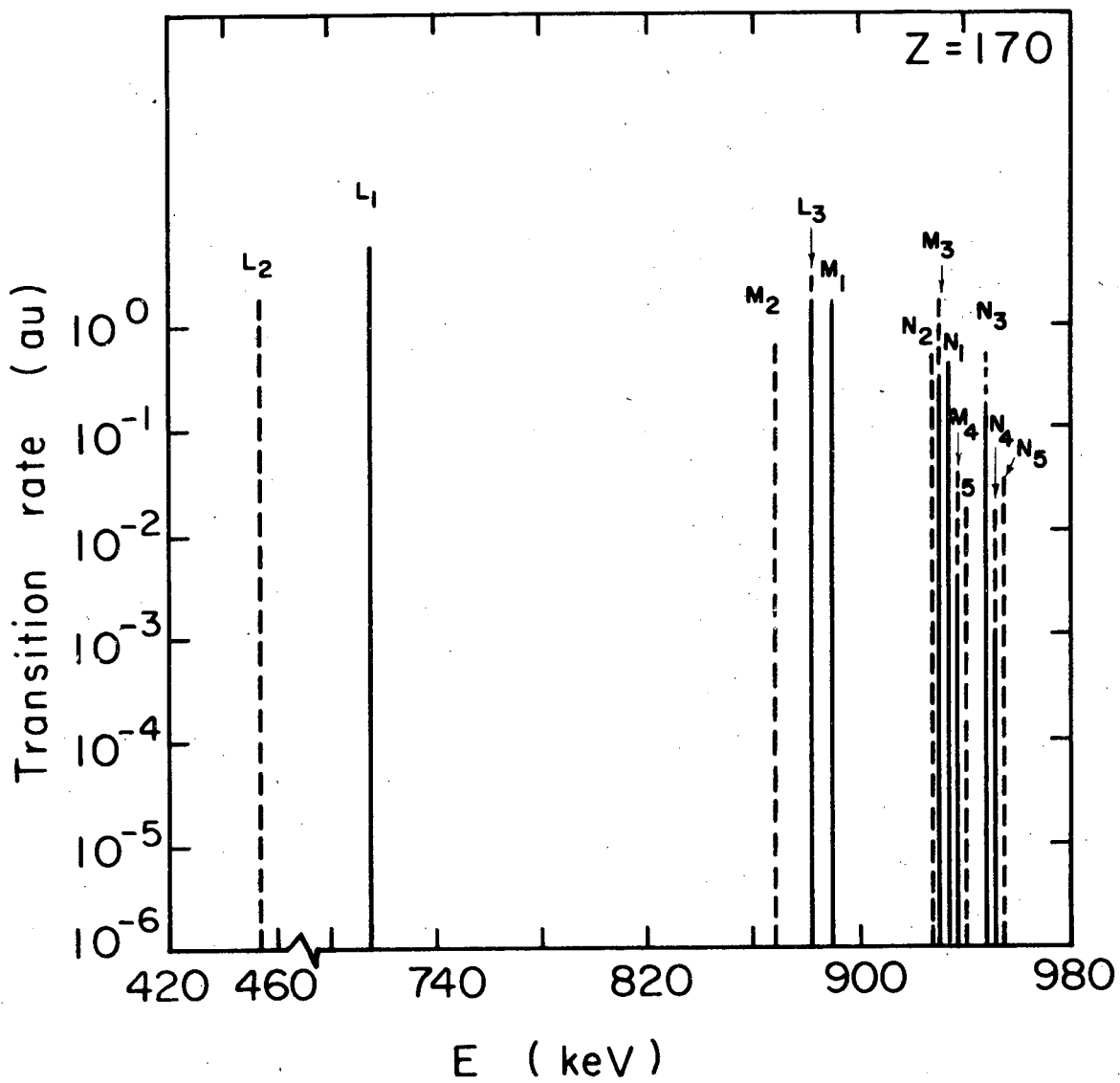
XBL738 - 3718

Fig. 5



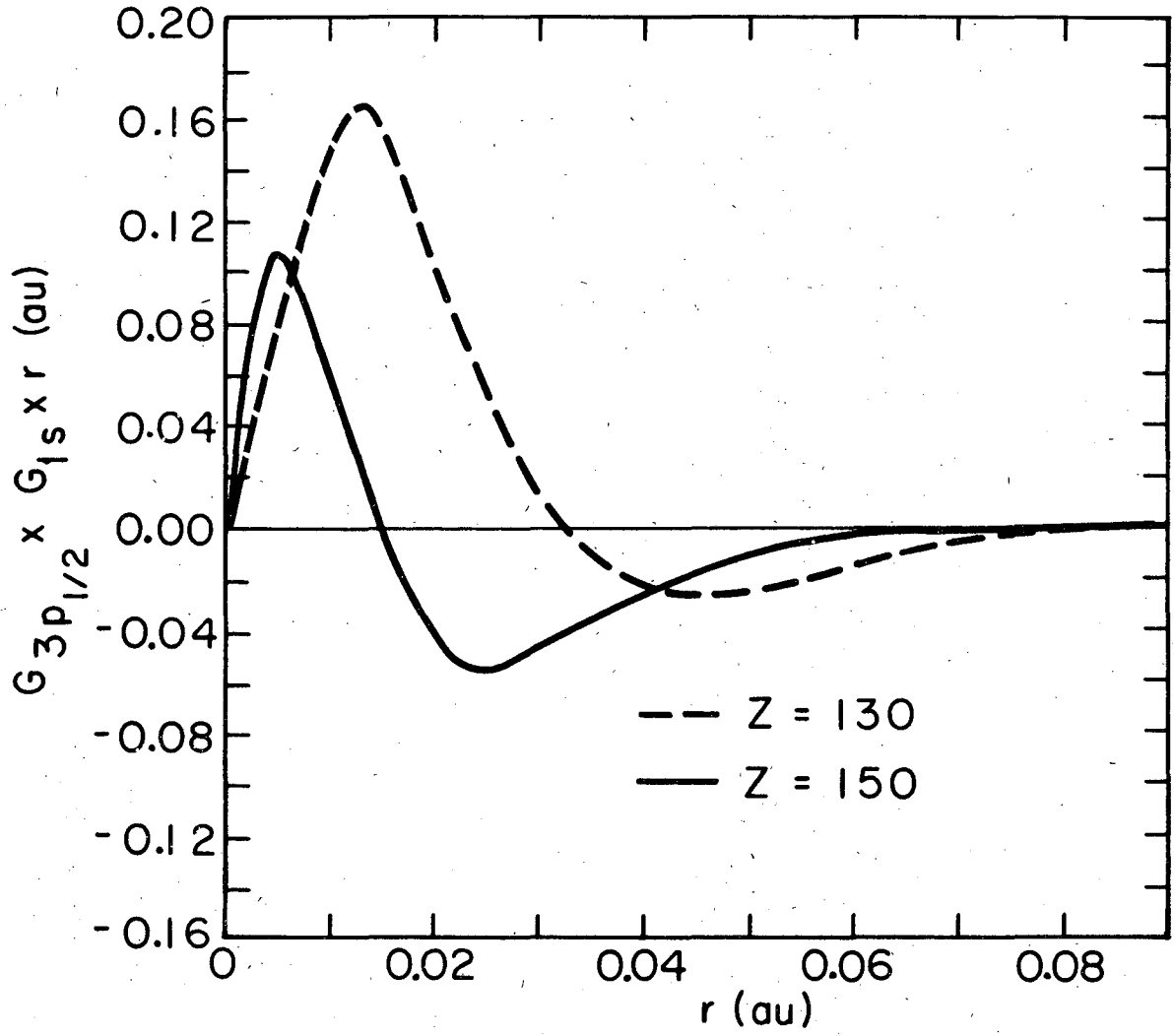
XBL738-3719

Fig. 6



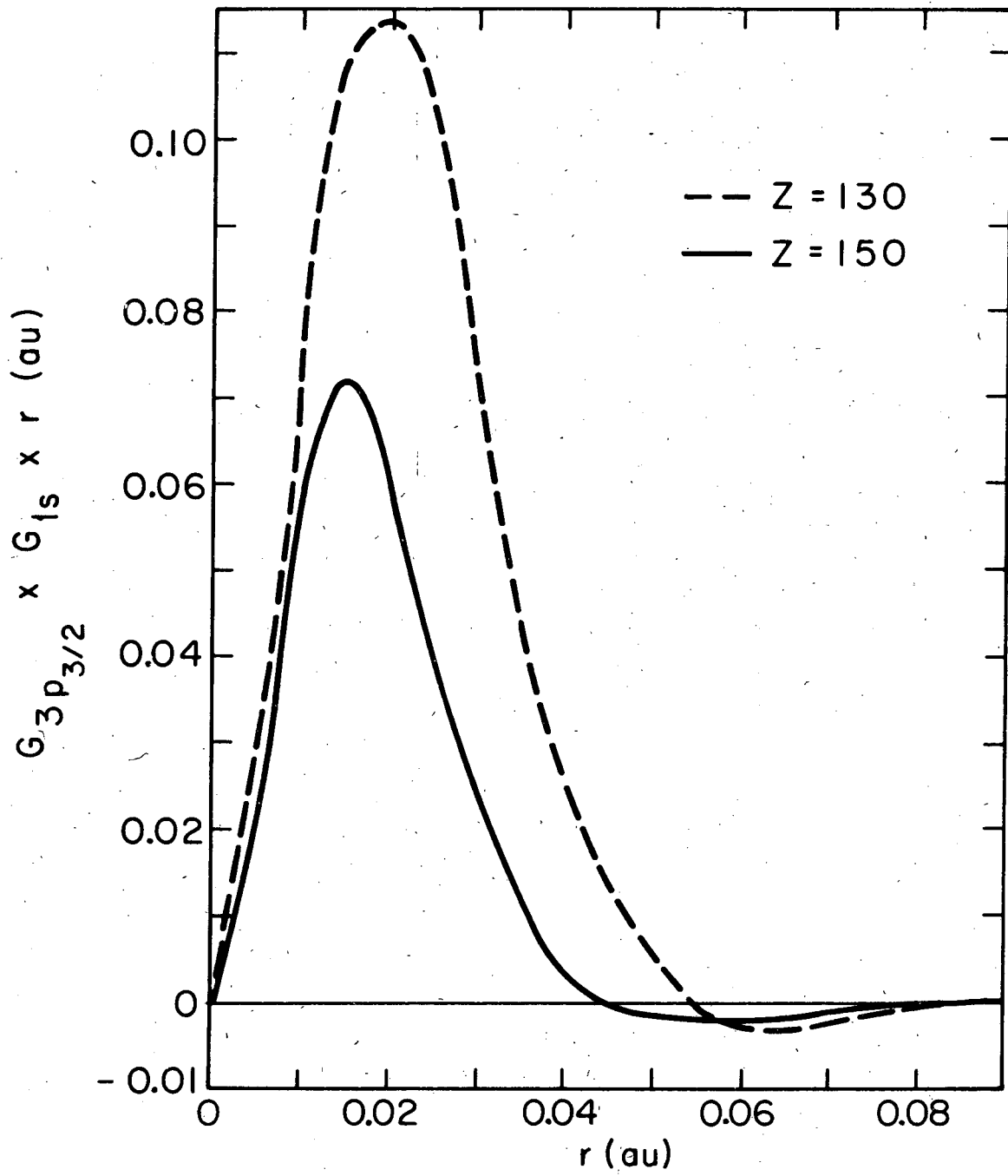
XBL738-3717

Fig. 7



XBL738-3715

Fig. 8



XBL738-3714

Fig. 9

LEGAL NOTICE

This report was prepared as an account of work sponsored by the United States Government. Neither the United States nor the United States Atomic Energy Commission, nor any of their employees, nor any of their contractors, subcontractors, or their employees, makes any warranty, express or implied, or assumes any legal liability or responsibility for the accuracy, completeness or usefulness of any information, apparatus, product or process disclosed, or represents that its use would not infringe privately owned rights.

TECHNICAL INFORMATION DIVISION
LAWRENCE BERKELEY LABORATORY
UNIVERSITY OF CALIFORNIA
BERKELEY, CALIFORNIA 94720